

Dependence of protein mechanical unfolding pathways on pulling speeds

Mai Suan Li and Maksim Kouza

*Institute of Physics, Polish Academy of Sciences,
Aleja Lotnikow 32/46, 02-668 Warszawa, Poland*

Abstract

Mechanical unfolding of the fourth domain of *Distyostelium discoideum* filamin (DDFLN4) was studied in detail using the C_α -Go model. We show that unfolding pathways of this protein depend on the pulling speed. The agreement between theoretical and experimental results on the sequencing of unfolding events is achieved at low loading rates. The unfolding free energy landscape is also constructed using dependencies of unfolding forces on pulling speeds.

I. INTRODUCTION

The last ten years have witnessed an intense activity in single-molecule force spectroscopy experiments in detecting inter and intramolecular forces of biological systems to understand their functions and structures. Much of the research has been focused on elastic properties of proteins, DNA, and RNA, i.e, their response to an external force, following the seminal papers by Rief *et al.* [1], and Tskhovrebova *et al.* [2]. The main advantage of this technique is its ability to separate out the fluctuations of individual trajectories from the ensemble average behavior observed in traditional bulk biochemical experiments. This allows for studying unfolding pathways in detail using the end-to-end distance as a reaction coordinate. Moreover, the single-molecule force spectroscopy can be used to decipher the unfolding free energy landscape (FEL) of biomolecules [3, 4].

As cytoskeletal proteins, large actin-binding proteins play a key roles in cell organization, mechanics and signalling[5]. During the process of permanent cytoskeleton reorganization, all involved participants are subject to mechanical stress. One of them is the fourth domain *Dictyostelium discoideum* filamin (DDFLN4), which binds different components of actin-binding protein. Therefore, understanding the mechanical response of this domain to a stretched force is of great interest. Recently, using the AFM experiments, Schwaiger *et al.* [6, 7] have obtained two major results for DDFLN4. First, this domain (Fig. 1) unfolds via intermediates as the force-extension curve displays two peaks centered at the end-to-end extension $\Delta R \approx 12$ nm and $\Delta R \approx 22$ nm. Second, with the help of loop mutations, it was suggested that during the first unfolding event (first peak) strands A and B unfold first. Therefore, strands C - G form a stable intermediate structure, which then unfolds in the second unfolding event (second peak). In addition, Schwaiger *et al.* [7] have also determined the FEL parameters of DDFLN4.

With the help of the C_α -Go model [8], Li *et al.* [4] have demonstrated that the mechanical unfolding of DDFLN4 does follow the three-state scenario but the full agreement between theory and experiments was not obtained. The simulations [4] showed that two peaks in the force-extension profile occur at $\Delta R \approx 1.5$ nm and 11 nm, i.e., the Go modeling does not detect the peak at $\Delta R \approx 22$ nm. Instead, it predicts the existence of a peak not far from the native conformation. More importantly, theoretical unfolding pathways [4] are very different from the experimental ones [6]: the unfolding initiates from the C-terminal, but not from

the N-terminal terminal as shown by the experiments.

It should be noted that the pulling speed used in the previous simulations is about five orders of magnitude larger than the experimental value [6]. Therefore, a natural question emerges is if the discrepancy between theory and experiments is due to huge difference in pulling speeds. Motivated by this, we have carried low- v simulations, using the Go model [8]. Interestingly, we uncovered that unfolding pathways of DDFLN4 depend on the pulling speed and only at $v \sim 10^4$ nm/s, the theoretical unfolding sequencing coincides with the experimental one [6]. However, even at low loading rates, the existence of the peak at $\Delta R \approx 1.5$ nm remains robust and the Go modeling does not capture the maximum at $\Delta R \approx 22$ nm.

In the previous work [4], using dependencies of unfolding times on external forces, the distance between the native state (NS) and intermediate state (IS) x_{u1} , and the distance between the IS and denaturated state (DS) x_{u2} of DDFLN4 have been estimated. In the Bell approximation, the agreement between the theory and experiments [7] was reasonable. However, in the non-Bell approximation [9], the theoretical values of x_{u1} , and x_{u2} seem to be high [4]. In addition the unfolding barrier between the first transition state (TS1) and NS ΔG_1^\ddagger is clearly higher than its experimental counterpart (Table 1).

In this paper, assuming that the microscopic kinetic theory [9] holds for a three-state protein, we calculated $x_{ui}(i = 1, 2)$ and unfolding barriers by a different method which is based on dependencies of peaks in the force-extension curve on v . Our present estimations for the unfolding FEL parameters are more reasonable compared to the previous ones [4]. Finally, we have also studied thermal unfolding pathways of DDFLN4 and shown that the mechanical unfolding pathways are different from the thermal ones.

II. METHOD

The native conformation of DDFLN4, which has seven β -strands, enumerated as A to G, was taken from the PDB (PI: 1KSR, Fig. 1a). We assume that residues i and j are in native contact if the distance between them in the native conformation, is shorter than a cutoff distance $d_c = 6.5$ Å. With this choice of d_c , the molecule has 163 native contacts. Native contacts exist between seven pairs of β -strands P_{AB} , P_{AF} , P_{BE} , P_{CD} , P_{CF} , P_{DE} , and P_{FG} (Fig. 1b).

We used the C_α -Go model [8] for a molecule. The corresponding parameters of this model are chosen as follows [10, 11]: $K_r = 100\epsilon_H/\text{\AA}^2$, $K_\theta = 20\epsilon_H/\text{rad}^2$, $K_\phi^{(1)} = \epsilon_H$, and $K_\phi^{(3)} = 0.5\epsilon_H$, where ϵ_H is the characteristic hydrogen bond energy, and $C = 4 \text{\AA}$. As in our previous works [10, 11], we set $\epsilon_H = 0.98 \text{ kcal/mol}$. Then, the temperature $T = 285 \text{ K}$ corresponds to $0.53\epsilon_H/k_B$ and all computations have been performed at this temperature. The force unit is $[f] = \epsilon_H/\text{\AA} = 68 \text{ pN}$ [10].

The simulations were carried out in the over-damped limit with the water viscosity $\zeta = 50 \frac{m}{\tau_L}$ [12], where the time unit $\tau_L = (ma^2/\epsilon_H)^{1/2} \approx 3 \text{ ps}$, m is a typical mass of amino-acids, and $a = 4 \text{\AA}$ a distance between two neighboring residues. Neglecting the inertia term, the Brownian dynamics equation was numerically solved by the simple Euler method. Due to the large viscosity, we can choose a large time step $\Delta t = 0.1\tau_L$, and this choice allows us to study unfolding at low loading rates.

In the constant velocity force simulations, we fix the N-terminal and pull the C-terminal by applying the force $f = K_r(\nu t - r)$, where r is the displacement of the pulled atom from its original position [13], and the spring constant of cantilever K_r is set to be the same as the spring constant of the Go model. The pulling direction was chosen along the vector drawn from the fixed atom to the pulled one.

The mechanical unfolding sequencing was studied by monitoring the fraction of native contacts of the β -strands and of their seven pairs as a function of ΔR , which is admitted a good reaction coordinate. In order to probe thermal unfolding pathways, for the i -th trajectory we introduce the progress variable $\delta_i = t/\tau_u^i$, where τ_u^i is the unfolding time [10]. Then one can average the fraction of native contacts over many trajectories in a unique time window $0 \leq \delta_i \leq 1$ and monitor the unfolding sequencing with the help of the progress variable δ .

III. RESULTS

A. Robustness of peak at $\Delta R \approx 1.5 \text{ nm}$ and absence of maximum at $\Delta R \approx 22 \text{ nm}$ at low pulling speeds

In our previous high pulling speed ($v = 3.6 \times 10^7 \text{ nm/s}$) simulations [4], the force-extension curve shows two peaks at $\Delta R \approx 1.5 \text{ nm}$ and 10 nm , while the experiments showed

that peaks appear at $\Delta R \approx 12$ nm and 22 nm. The question we ask if one can reproduce the experimental results at low pulling speeds. Within our computational facilities, we were able to perform simulations at the lowest $v = 2.6 \times 10^4$ nm/s which is about three orders of magnitude lower than that used before [4].

Fig. 2 show force-extension curves for four representative pulling speeds. For the highest $v = 7.2 \times 10^6$ nm/s (Fig. 2a), there are two peaks located at extensions $\Delta R \approx 1.5$ nm and 9 nm. As evident from Figs. 2b, c and d, the existence of the first peak remains robust against reduction of v . Positions of f_{max1} weakly fluctuate over the range $0.9 \lesssim \Delta R \lesssim 1.8$ nm for all values of v (Fig. 3). As v is reduced, f_{max1} decreases but this peak does not vanish if one interpolate our results to the lowest pulling speed $v_{exp} = 200$ nm/s used in the experiments [6] (see below). Thus, opposed to the experiments, the first peak occurs already at small end-to-end extensions. We do not exclude a possibility that such a peak was overlooked by experiments, as it happened with the titin domain I27. Recall that, for this domain the first AFM experiment [1] did not trace the hump which was observed in the later simulations [13] and experiments [14].

Positions of the second peak f_{max2} are more scattered compared to f_{max1} , ranging from about 8 nm to 12 nm (Fig. 3). Overall, they move toward higher values upon reduction of v (Fig. 2). If at $v = 6.4 \times 10^5$ nm/s only about 15% trajectories display $\Delta R_{max2} > 10$ nm, then this percentage reaches 65% and 97% for $v = 5.8 \times 10^4$ nm/s and 2.6×10^4 nm/s, respectively (Fig. 3).

At low v , unfolding pathways show rich diversity. For $v \gtrsim 6.4 \times 10^5$ nm/s, the force-extension profile shows only two peaks in all trajectories studied (Fig. 2a and 2b), while for lower speeds $v = 5.8 \times 10^4$ nm/s and 2.6×10^4 nm/s, about 4% trajectories display even four peaks (Fig. 2c and 2d), i.e. the four-state behavior.

We do not observe any peak at $\Delta R \approx 22$ nm for all loading rates (Fig. 2), and it is very unlikely that it will appear at lower values of v . Thus, the Go model, in which non-native interactions are neglected, fails to reproduce this experimental observation. Whether inclusion of non-native interactions would cure this problem requires further studies.

B. Dependence of mechanical unfolding pathways on loading rates

The considerable fluctuations of peak positions and occurrence of even three peaks already suggest that unfolding pathways, which are kinetic in nature, may change if v is varied. To clarify this point in more detail, we show ΔR -dependencies of native contacts of all β -strands and their pairs for $v = 7.2 \times 10^6$ nm/s (Fig. 4) and $v = 2.6 \times 10^4$ nm/s (Fig. 5). For $v = 7.2 \times 10^6$ nm/s, one has the following unfolding pathways:

$$G \rightarrow F \rightarrow (C, E, D) \rightarrow B \rightarrow A, \quad (1a)$$

$$P_{AF} \rightarrow P_{BE} \rightarrow (P_{FG}, P_{CF}) \rightarrow P_{CD} \rightarrow P_{DE} \rightarrow P_{AB}. \quad (1b)$$

According to this scenario, the unfolding initiates from the C-terminal, while the experiments [6] showed that strands A and B unfold first. For $v = 2.6 \times 10^4$ nm/s, Fig. 5 gives the following sequencing

$$(A, B) \rightarrow (C, D, E) \rightarrow (F, G), \quad (2a)$$

$$P_{AF} \rightarrow (P_{BE}, P_{AB}) \rightarrow P_{CF} \rightarrow (P_{CD}, P_{DE}, P_{FG}). \quad (2b)$$

We obtain the very interesting result that at this low loading rate, in agreement with the AFM experiments [6], the N-terminal detaches from a protein first.

For both values of v , the first peak corresponds to breaking of native contacts between strands A and F (Fig. 4b and Fig. 5b). However, the structure of unfolding intermediates, which correspond to this peak, depends on v . For $v = 7.2 \times 10^6$ nm/s (Fig. 4), at $\Delta R \approx 1.5$ nm, native contacts between F and G are broken and strand G has already been unstructured (Fig. 4a). Therefore, for this pulling speed, the intermediate consists of six ordered strands A-F (see Fig. 6a for a typical snapshot). In the $v = 2.6 \times 10^4$ nm/s case, just after the first peak, none of strands unfolds completely (Fig. 5a), although (A,F) and (B,E) contacts have been already broken (Fig. 5b). Thus, the intermediate looks very different from the high v case, as it has all secondary structures partially structured (see (Fig. 6b) for a typical snapshot). Since the experiments [6] showed that intermediate structures contain five ordered strands C-G, intermediates predicted by simulations are more ordered than the experimental ones. Even though, our low loading rate Go simulations provide the same pathways as on the experiments. The difference between theory and experiments in intermediate structures comes from different locations of the first peak. It remains unclear if

this is a shortcoming of Go models or of the experiments because it is hard to imagine that a β -protein like DDFLN4 displays the first peak at such a large extension $\Delta R \approx 12$ nm [6]. The force-extension curve of the titin domain I27, which has a similar native topology, for example, displays the first peak at $\Delta R \approx 0.8$ nm [14]. From this prospect, the theoretical result is more favorable.

The strong dependence of unfolding pathways on loading rates is also clearly seen from structures around the second peak. In the $v = 7.2 \times 10^6$ nm/s case, at $\Delta R \approx 11$ nm, strands A and B remain structured, while other strands detach from a protein core (Fig. 4 and Fig. 6c). This is entirely different from the low loading case, where A and B completely unfold but F and G still survive (Fig. 5 and Fig. 6d). The result, obtained for $v = 2.6 \times 10^4$ nm/s, is in full agreement with the experiments [6] that at $\Delta R \approx 12$ nm, A and B detached from the core.

Note that the unfolding pathways given by Eq. 1a, 1b, 2a, and 2b are valid in the statistical sense. In all 50 trajectories studied for $v = 7.2 \times 10^5$ nm/s, strands A and B always unfold last, and F and G unfold first (Eq. 1a), while the sequencing of unfolding events for C, D and E depends on individual trajectories. At $v = 2.6 \times 10^4$ nm/s, most of trajectories follow the pathway given by Eq. 2a, but we have observed a few unusual pathways, as it is illustrated in Fig. 7. Having three peaks in the force-extension profile, the evolution of native contacts of F and G display an atypical behavior. At $\Delta R \approx 7$ nm, these strands fully unfold (Fig. 7c), but they refold again at $\Delta R \approx 11$ nm (Fig. 7b and 7d). Their final unfolding takes place around $\Delta R \approx 16.5$ nm. As follows from Fig. 7b, the first peak in Fig. 7a corresponds to unfolding of G. Strands A and B unfold after passing the second peak, while the third maximum occurs due to unfolding of C-G, i.e. of a core part shown in Fig. 7d.

The dependence of unfolding pathways on v is understandable. If a protein is pulled very fast, the perturbation, caused by the external force, does not have enough time to propagate to the fixed N-terminal before the C-terminal unfolds. Therefore, at very high v , we have the pathway given by Eq. 1a. In the opposite limit, it does matter what end is pulled as the external force is uniformly felt along a chain. Then, a strand, which has a weaker link with the core, would unfold first.

C. Computation of FEL parameters

As mentioned above, at low loading rates, for some trajectories, the force-extension curve does not show two, but three peaks. However, the percentage of such trajectories is rather small, we will neglect them and consider DDFLN4 as a three-state protein. Recently, using dependencies of unfolding times on the constant external force and the non-linear kinetic theory [9], we obtained distances $x_{u1} \approx x_{u2} \approx 13\text{\AA}$ [4]. These values seem to be large for β -proteins like DDFLN4, which are supposed to have smaller x_u compared to α/β - and α -ones [15]. A clear difference between theory and experiments was also observed for the unfolding barrier ΔG_1^\ddagger . In order to see if one can improve our previous results, we will extract the FEL parameters by a different approach. Namely, assuming that all FEL parameters of the three-state DDFLN4, including the barrier between the second transition state and the intermediate state ΔG_2^\ddagger (see Ref. 4 for the definition), can be determined from dependencies of f_{max1} and f_{max2} on v , we calculate them in the the Bell-Evans-Rirchie approximation as well as beyond this approximation.

Estimation of x_{u1} and x_{u2} in the Bell-Evans-Rirchie approximation

In this approximation, x_{u1} and x_{u2} are related to v , f_{max1} and f_{max2} by the following equation [16]:

$$f_{maxi} = \frac{k_B T}{x_{ui}} \ln \left[\frac{v x_{ui}}{k_{ui}(0) k_B T} \right], i = 1, 2, \quad (3)$$

where $k_{ui}(0)$ is unfolding rates at zero external force. In the low force regime ($v \lesssim 2 \times 10^6$ nm/s), the dependence of f_{max} on v is logarithmic and x_{u1} and x_{u2} are defined by slopes of linear fits in Fig. 8. Their values are listed in Table 1. The estimate of x_{u2} agrees very well with the experimental [7] as well as with the previous theoretical result [4]. The present value of x_{u1} agrees with the experiments better than the old one [4]. Presumably, this is because it has been estimated by the same procedure as in the experiments [7].

It is important to note that the logarithmic behavior is observed only at low enough v . At high loading rates, the dependence of f_{max} on v becomes power-law. This explains why all-atom simulations, performed at $v \sim 10^9$ nm/s for most of proteins, are not able to provide reasonable estimations for x_u .

The another interesting question is if the peak at $\Delta R \approx 1.5$ nm disappears at loading rates used in the experiments [7]. Assuming that the logarithmic dependence in Fig. 8 has the same slope at low v , we interpolate our results to $v_{exp} = 200$ nm/s and obtain

$f_{max1}(v_{exp}) \approx 40$ pN. Thus, in the framework of the Go model, the existence of the first peak is robust at experimental speeds.

Beyond the Bell-Evans-Rirchie approximation

In the Bell-Evans-Rirchie approximation, one assumes that the location of the transition state does not move under the action of an external force. However, our simulations for ubiquitin, for example, showed that it does move toward the NS [10]. Recently, assuming that x_u depends on the external force and using the Kramers theory, Dudko *et al.* have tried to go beyond the Bell-Evans-Rirchie approximation. They proposed [9] the following formula for dependence of the unfolding force on x_u and v :

$$f_{max} = \frac{\Delta G^\ddagger}{\nu x_u} \left\{ 1 - \left[\frac{k_B T}{\Delta G^\ddagger} \ln \frac{k_B T k_u(0) e^{\Delta G^\ddagger / k_B T + \gamma}}{x_u v} \right]^\nu \right\} \quad (4)$$

Here, ΔG^\ddagger is the unfolding barrier, $\nu = 1/2$ and $2/3$ for the cusp [17] and the linear-cubic free energy surface [18], respectively. $\gamma \approx 0.577$ is the Euler-Mascheroni constant. Note that $\nu = 1$ corresponds to the phenomenological Bell theory (Eq. 3). If $\nu \neq 1$, then Eq. 4 can be used to estimate not only x_u , but also G^\ddagger . Since the fitting with $\nu = 1/2$ is valid in a wider force interval compared to the $\nu = 2/3$ case, we consider the former case only. The region, where the $\nu = 1/2$ fit works well, is expectantly wider than that for the Bell scenario (Fig. 8). From the nonlinear fitting (Eq. 4), we obtain $x_{u1} = 7.0\text{\AA}$, and $x_{u2} = 9.7\text{\AA}$ which are about twice as large as the Bell estimates (Table 1). Using AFM data, Schlierf and Rief [19], have shown that beyond Bell-Evans-Rirchie approximation $x_u \approx 11\text{\AA}$. This value is close to our estimate for x_{u2} . However, a full comparison with experiments is not possible as these authors did not consider x_{u1} and x_{u2} separately. The present estimations of these quantities are clearly lower than the previous one [4] (Table 1). The lower values of x_u would be more favorable because they are expected to be not high for beta-rich proteins [15] like DDFLN4. Thus, beyond Bell-Evans-Rirchie approximation, the method based on Eq. 4 provides more reasonable estimations for x_{ui} compared to the method, where these parameters are extracted from unfolding rates [4]. However, in order to decide what method is better, more experimental studies are required.

The corresponding values for G_1^\ddagger , and G_2^\ddagger are listed in Table 1. The experimental and previous theoretical results [4] are also shown for comparison. The present estimates for both barriers agree with the experimental data, while the previous theoretical value of ΔG_1^\ddagger fits to experiments worse than the current one.

D. Thermal unfolding pathways

In order to see if the thermal unfolding pathways are different from the mechanical ones, we performed zero-force simulations at $T = 410$ K. The progress variable δ is used as a reaction coordinate to monitor pathways (see *Materials and Methods*). From Fig. 9, we have the following sequencing for strands and their pairs:

$$G \rightarrow (B, C, E) \rightarrow (A, F, D), \quad (5a)$$

$$P_{AF} \rightarrow P_{BE} \rightarrow (P_{CD}, P_{CF}) \rightarrow (P_{AB}, P_{FG}, P_{DE}). \quad (5b)$$

It should be noted that these pathways are just major ones as other pathways are also possible. The pathway given by Eq. 5b, e.g., occurs in 35% of events. About 20% of trajectories follow $P_{AF} \rightarrow P_{CF} \rightarrow P_{BE} \rightarrow (P_{CD}, P_{AB}, P_{FG}, P_{DE})$ scenario. We have also observed the sequencing $P_{AF} \rightarrow P_{BE} \rightarrow (P_{CF}, P_{AB}, P_{FG}, P_{DE}) \rightarrow P_{CD}$, and $P_{BE} \rightarrow P_{AF} \rightarrow (P_{CD}, P_{CF}, P_{AB}, P_{FG}, P_{DE})$ in 12% and 10% of runs, respectively. Thus, due to strong thermal fluctuations, thermal unfolding pathways are more diverse compared to mechanical ones. From Eqs. 1a, 1b, 2a, 2b, 5a, and 5b, it is clear that thermal unfolding pathways of DDFLN4 are different from the mechanical pathways. This is also illustrated in Fig. 9c. As in the mechanical case (Fig. 6a and 6b), the contact between A and F is broken, but the molecule is much less compact at the same end-to-end distance. Although 7 contacts ($\approx 64\%$) between strands F and G remain survive, all contacts of pairs P_{AF} , P_{BE} and P_{CD} are already broken.

The difference between mechanical and thermal unfolding pathways is attributed to the fact that thermal fluctuations have a global effect on the biomolecule, while the force acts only on its termini. Such a difference was also observed for other proteins like I27 [20] and ubiquitin [10, 21]. We have also studied folding pathways of DDFLN4 at $T = 285$ K. It turns out that they are reverse of the thermal unfolding pathways given by Eqs. 5a and 5b. It would be interesting to test our prediction on thermal folding/unfolding of this domain experimentally.

Conclusions

The key result of this paper is that mechanical unfolding pathways of DDFLN4 depend on loading rates. At large v the C-terminal unfolds first, but the N-terminal unfolds at low $v \sim 10^4$ nm/s. The agreement with the experiments [6] is obtained only in low loading rate

simulations. The dependence of mechanical unfolding pathways on the loading rates was also observed for I27 (M.S. Li, unpublished). On the other hand, the previous studies [10, 22] showed that mechanical unfolding pathways of the two-state ubiquitin do not depend on the force strength. Since DDFLN4 and I27 are three-state proteins, one may think that the unfolding pathway change with variation of the pulling speed, is universal for proteins that unfold via intermediates. A more comprehensive study is needed to verify this interesting issue.

Dependencies of unfolding forces on pulling speeds have been widely used to probe FEL of two-state proteins [23]. However, to our best knowledge, here we have made a first attempt to apply this approach to extract not only x_{ui} , but also ΔG_i^\ddagger ($i = 1, \text{ and } 2$) for a three-state protein. This allows us to improve our previous results [4]. More importantly, a better agreement with the experimental data [7, 19] suggests that this method is also applicable to other multi-state biomolecules. Our study clearly shows that the low loading rate regime, where FEL parameters can be estimated, occurs at $v \leq 10^6$ nm/s which are about two-three orders of magnitude lower than those used in all-atom simulations. Therefore, at present, deciphering unfolding FEL of long proteins by all-atom simulations with explicit water is computationally prohibited. From this point of view, coarse-grained models are of great help.

We predict the existence of a peak at $\Delta R \sim 1.5$ nm even at pulling speeds used in now a day experimental setups. One of possible reasons of why the experiments did not detect this maximum is related to a strong linker effect as a single DDFLN4 domain is sandwiched between Ig domains I27-30 and domains I31-34 from titin [6]. Therefore, our result would stimulate new experiments on mechanical properties of this protein. Capturing the experimentally observed peak at $\Delta R \sim 22$ nm remains a challenge to theory.

Mechanical unfolding pathways of DDFLN4 and other proteins [10, 20, 21] are different from thermal ones. In accord with a common belief [24], thermal unfolding pathways of these proteins were shown to be reverse of folding pathways. Therefore, their folding mechanisms can not be gained from mechanical studies. Recently, using the all-atom simulations with implicit solvent [25], it has been found that a 49-residue C-terminal of TOP7 (residues 2-50 of 2GJH.pdb) folds via a non-trivial caching mechanism [26] and its thermal unfolding pathways are not reverse of the folding ones [27]. Can the folding mechanism of this fragment be deduced from mechanical unfolding simulations and experiments? A detailed study of this

interesting question is in progress but our preliminary simulation results show that folding pathways may be inferred from the mechanical ones.

The work was supported by the Ministry of Science and Informatics in Poland (grant No 202-204-234). MK is very grateful to the Polish committee for UNESCO for the financial support.

-
- [1] M. Rief, M. Gautel, F. Oesterhelt, J. M. Fernandez and H. E. Gaub, *Science* **276**, 1109 (1997)
- [2] L. Tskhovrebova, K. Trinick, J. A. Sleep and M. Simons, *Nature* **387**, 308 (1997)
- [3] C. Bustamante, Y. R. Chemla, N. R. Forde and D. Izhaky, *Annu. Rev. Biochem.* **73**, 705 (2004)
- [4] M. S. Li, A. M. Gabovich and A. I. Voitenko, *J. Chem. Phys.* **128**, 045103 (2008)
- [5] T. P. Stossel, J. Condeelis, L. Cooley, J. H. Hartwig, A. Noegel, M. Schleicher and S.S. Shapiro, *Nat Rev Mol Cell Biol.* **2**, 138 (2001)
- [6] I. Schwaiger, A. Kardinal, M. Schleicher, A. A. Noegel and M. Rief, *Nat. Struct. Mol. Biol.* **11**, 81 (2004)
- [7] I. Schwaiger, M. Schlierf, A.A. Noegel and M. Rief, *EMBO reports* **6**, 46 (2005)
- [8] C. Clementi, H. Nymeyer and J. N. Onuchic, *J. Mol. Biol.* **298**, 937 (2000)
- [9] O. K. Dudko, G. Hummer and A. Szabo, *Phys. Rev. Lett.* **96**, 108101 (2006)
- [10] M. S. Li, M. Kouza and C. K. Hu, *Biophys. J.* **92**, 547 (2007)
- [11] M. Kouza, C. K. Hu and M. S. Li, *J. Chem. Phys.* **128**, 045103 (2008)
- [12] T. Veitshans, D. K. Klimov and D. Thirumalai, *Folding and Design* **2**, 1 (1997)
- [13] H. Lu, B. Isralewitz, A. Krammer, V. Vogel and K. Schulten, *Biophys. J.* **75**, 662 (1998)
- [14] P. E. Marszalek, H. Lu, H. B. Li, M. Carrion-Vazquez, A. F. Oberhauser, K. Schulten and J. M. Fernandez, *Nature* **402**, 100 (1999)
- [15] M. S. Li, *Biophys. J.* **93**, 2644 (2007)
- [16] E. Evans and K. Ritchie, *Biophys. J.* **72**, 1541 (1997)
- [17] G. Hummer and A. Szabo, *Biophys. J.* **85**, 5 (2003)
- [18] O. K. Dudko, A. E. Filippov, J. Klafter and U. Urbakh, *PNAS* **100**, 11378 (2003)
- [19] M. Schlierf and M. Rief, *Biophys. J.* **90**, L33 (2006)
- [20] E. Paci and M. Karplus, *Proc. Natl. Acad. Sci. USA* **97**, 6521 (2000)
- [21] S. Mitternacht and A. Irback, *Proteins: Structures, Functions, and Bioinformatics* **65**, 759 (2006)
- [22] A. Irback, S. Mitternacht and S. Mohanty, *Proc. Natl. Acad. Sci. USA* **102**, 13427 (2005)
- [23] R. B. Best, S. B. Fowler, J. L. Toca-Herrera and J. Clarke, *PNAS* **99**, 12143 (2002)
- [24] V. Daggett and A. Fersht, *Trends Biochem. Sci.* **28**, 18 (2003).

- [25] A. Irback and S. Mohanty, *J. Com. Chem.* **27**, 1548 (2006)
- [26] S. Mohanty, J. H. Meinke, O. Zimmermann, and U.H.E. Hansmann, *Proc. Natl. Acad. Sci. USA* **105**, 8004 (2008).
- [27] S. Mohanty, and U.H.E. Hansmann, *J. Phys. Chem. B* **112**, 15134 (2008).

	Bell approximation		Beyond Bell approximation			
	$x_{u1}(\text{\AA})$	$x_{u2}(\text{\AA})$	$x_{u1}(\text{\AA})$	$x_{u2}(\text{\AA})$	$\Delta G_1^\ddagger/k_B T$	$\Delta G_2^\ddagger/k_B T$
Theory [4]	6.3 ± 0.2	5.1 ± 0.2	13.1	12.6	25.8	18.7
Theory (this work)	3.2 ± 0.2	5.5 ± 0.2	7.0	9.7	19.9	20.9
Exp. [7, 19]	4.0 ± 0.4	5.3 ± 0.4			17.4	17.2

Table 1. Parameters x_{u1} , and x_{u2} were obtained in the Bell and beyond-Bell approximation. Theoretical values of the unfolding barriers were extracted from the microscopic theory of Dudko *et al* (Eq. 4) with $\nu = 1/2$. The experimental estimates were taken from Ref. 4.

Figure Captions

FIGURE 1. (a) Native state conformation of DDFLN4 taken from the PDB (PDB ID: 1ksr). There are seven β -strands: A (6-9), B (22-28), C (43-48), D (57-59), E (64-69), F (75-83), and G (94-97). In the native state there are 15, 39, 23, 10, 27, 49, and 20 native contacts formed by strands A, B, C, D, E, F, and G with the rest of the protein, respectively. The end-to-end distance in the native state $R_{NS} = 40.2 \text{ \AA}$. (b) There are 7 pairs of strands, which have the nonzero number of mutual native contacts in the native state. These pairs are P_{AB} , P_{AF} , P_{BE} , P_{CD} , P_{CF} , P_{DE} , and P_{FG} . The number of native contacts between them are 11, 1, 13, 2, 16, 8, and 11, respectively.

FIGURE 2. Typical force-extension curves for $v = 7.2 \times 10^6 \text{ nm/s}$ (a), $6.4 \times 10^5 \text{ nm/s}$ (b), $5.8 \times 10^4 \text{ nm/s}$ (c), and $2.6 \times 10^4 \text{ nm/s}$ (d). The arrow in (c) and (d) roughly refers to locations of additional peaks for two trajectories (red and green).

FIGURE 3. Distributions of positions of f_{max1} and f_{max2} for $v = 7.2 \times 10^6$ (solid), 6.4×10^5 (dashed), 5.8×10^4 (dotted) and $2.6 \times 10^4 \text{ nm/s}$ (dashed-dotted).

FIGURE 4. (a) Dependence of averaged fractions of native contacts formed by seven strands on ΔR for $v = 7.2 \times 10^6 \text{ nm/s}$. (b) The same as in (a) but for pairs of strands. Arrows refer to the positions of peaks. Results were averaged over 50 trajectories.

FIGURE 5. The same as in Fig. 4 but for $v = 2.6 \times 10^4 \text{ nm/s}$. Results were averaged over 50 trajectories.

FIGURE 6. (a) Typical snapshot obtained at $\Delta R = 2 \text{ nm}$ and $v = 7.2 \times 10^6 \text{ nm/s}$. A single contact between strand A (blue spheres) and strand F (orange) was broken (dotted lines). Native contacts between F and G (red) are also broken and G completely unfolds. (b) The same as in (a) but for $v = 2.6 \times 10^4 \text{ nm/s}$. Native contacts between A and F and between B and E are broken (dotted lines), but all strands are remain partially structured. (c) Typical snapshot obtained at $\Delta R = 11 \text{ nm}$ and $v = 7.2 \times 10^6 \text{ nm/s}$. Native contacts between pairs are broken except those between strands A and B. All 11 unbroken contacts are marked by solid lines. Strands A and B do not unfold yet. (d) The same as in (c) but for $v = 2.6 \times 10^4 \text{ nm/s}$. Two from 11 native contacts between F and G are broken (dotted

lines). Contacts between other pairs are already broken, but F and G remain structured.

FIGURE 7. (a) Force-extension curve for an anomalous unfolding pathway at $v = 2.6 \times 10^4$ nm/s. (b) Dependence of fractions of native contacts of seven strands on ΔR . Snapshot at $\Delta R = 7.4$ nm (c) and $\Delta R = 11$ nm (d).

FIGURE 8. Dependence of f_{max1} (open circles) and f_{max2} (open squares) on v . The values of these peaks were obtained as averages over all trajectories. The arrow separates the low pulling speed regime from the high one. Straight lines are fits to the Bell-Evans-Rirchie equation ($y = -20.33 + 11.424 \ln(x)$ and $y = 11.54 + 6.528 \ln(x)$ for F_{max1} and F_{max2} , respectively). Here f_{max} and v are measured in pN and nm/s, respectively. From these fits we obtain $x_{u1} = 3.2 \text{ \AA}$ and $x_{u2} = 5.5 \text{ \AA}$. The solid circle and triangle correspond to $f_{max1} \approx 40$ pN and $f_{max2} \approx 46$ pN, obtained by interpolation of linear fits to the experimental value $v = 200$ nm/s. Fitting to the nonlinear microscopic theory (dashed lines) gives $x_{u1} = 7.0 \text{ \AA}$, $\Delta G_1^\ddagger = 19.9 k_B T$, $x_{u2} = 9.7 \text{ \AA}$, and $\Delta G_2^\ddagger = 20.9 k_B T$.

FIGURE 9. Thermal unfolding pathways. (a) Dependence of native contact fractions of seven strands on the progress variable δ at $T = 410$ K. (b) The same as in (a) but for seven strand pairs. (c) A typical snapshot at $\Delta R \approx 1.8$ nm. The contact between strands A and F is broken (dotted lines) but 7 contacts between strands S6 and S7 (solid lines) still survive.

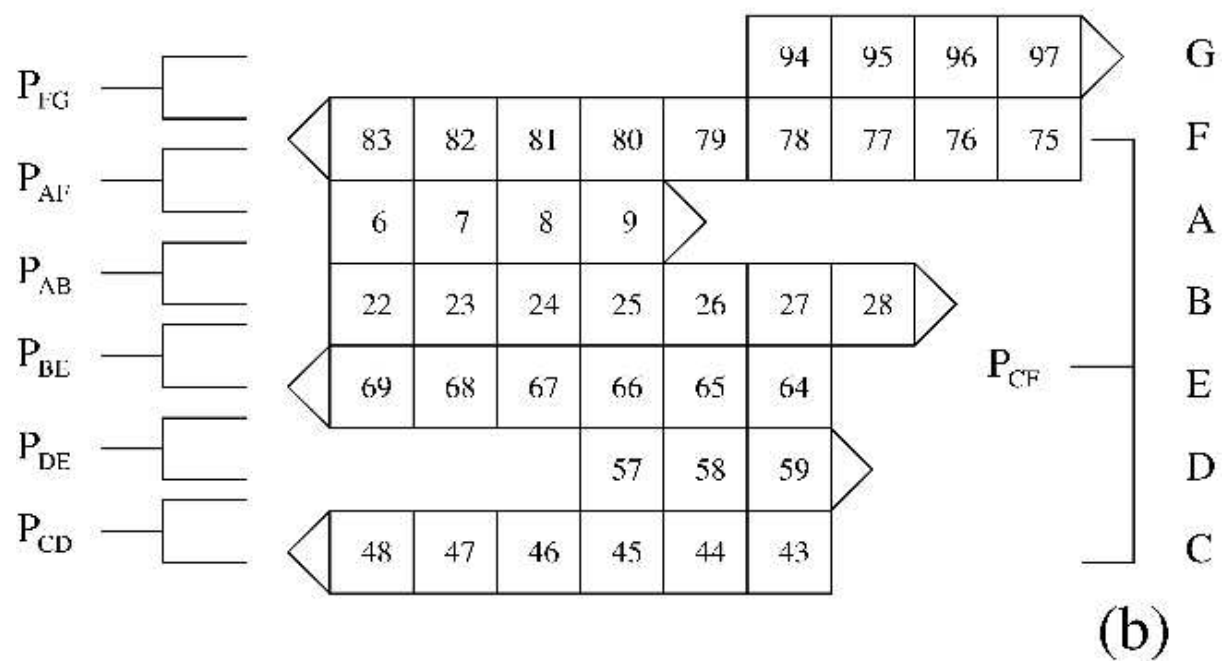
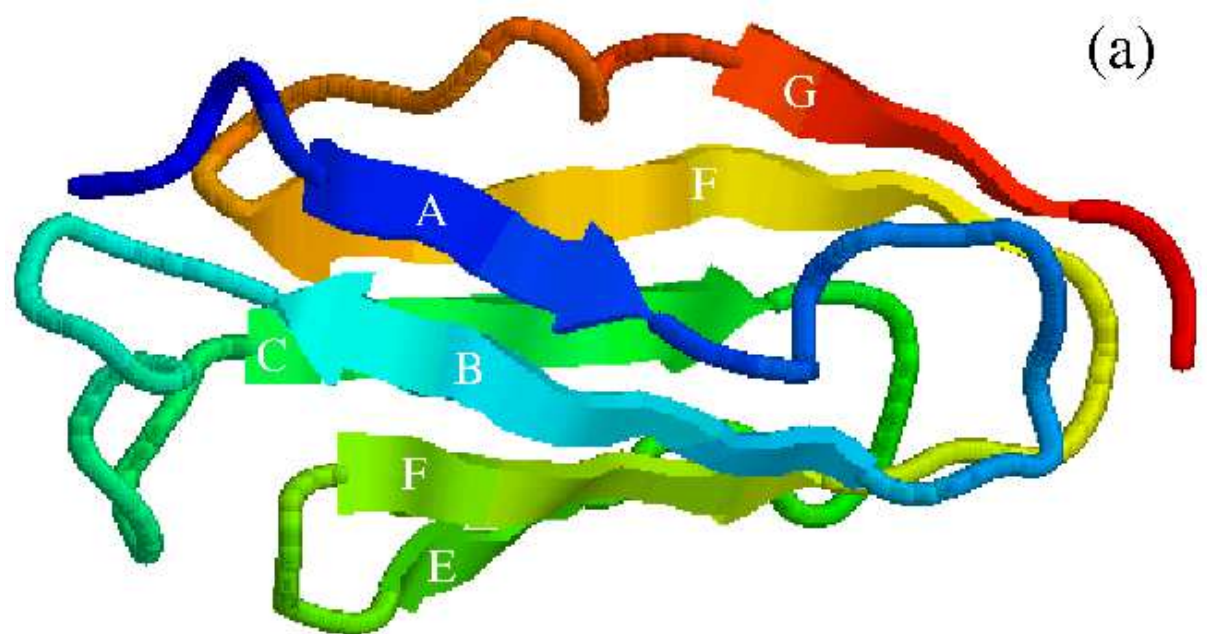


FIG. 1:

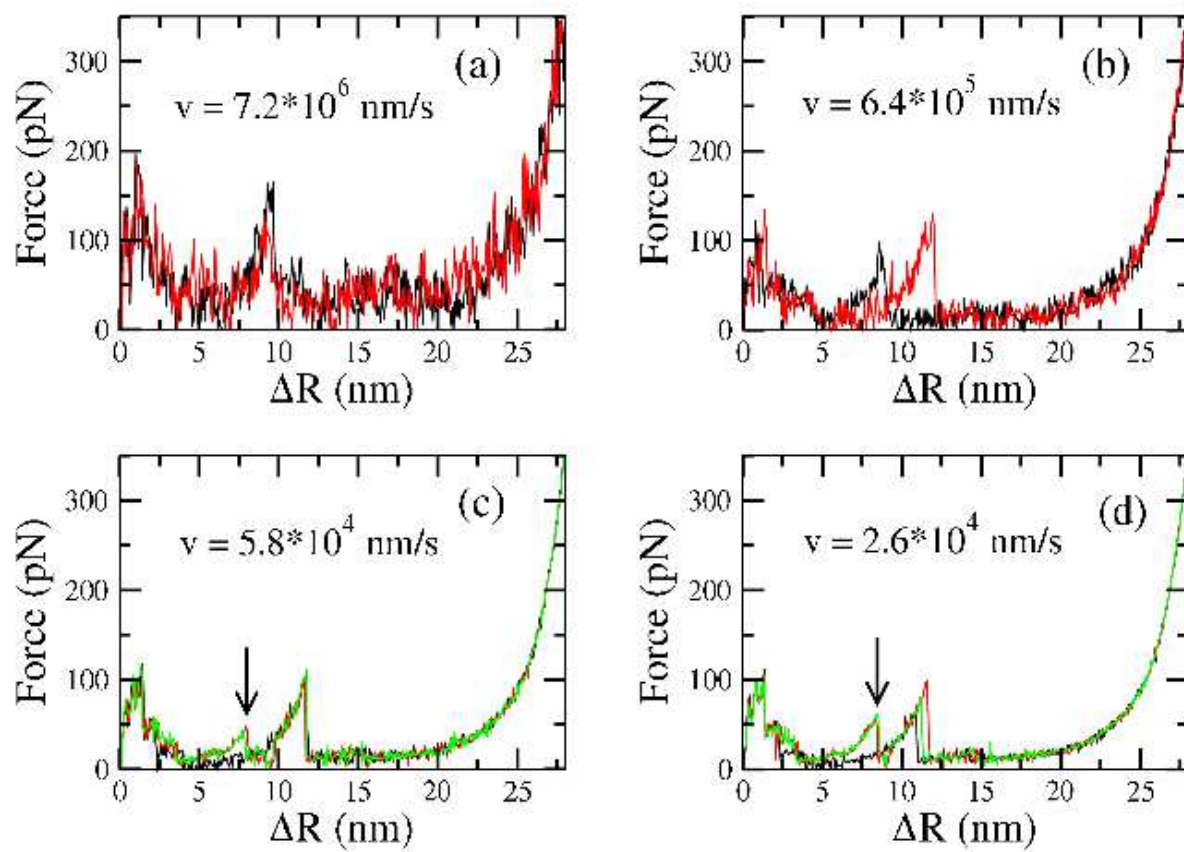


FIG. 2:

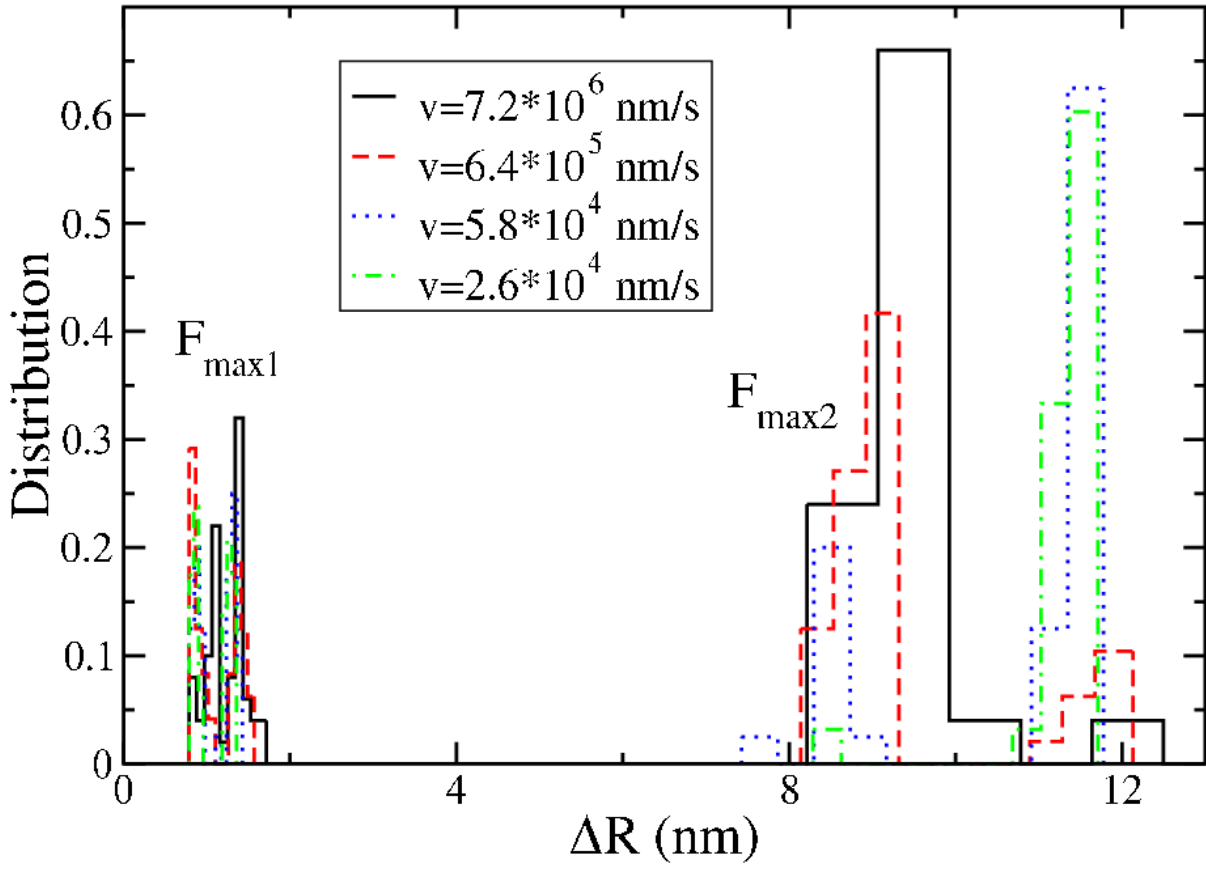


FIG. 3:

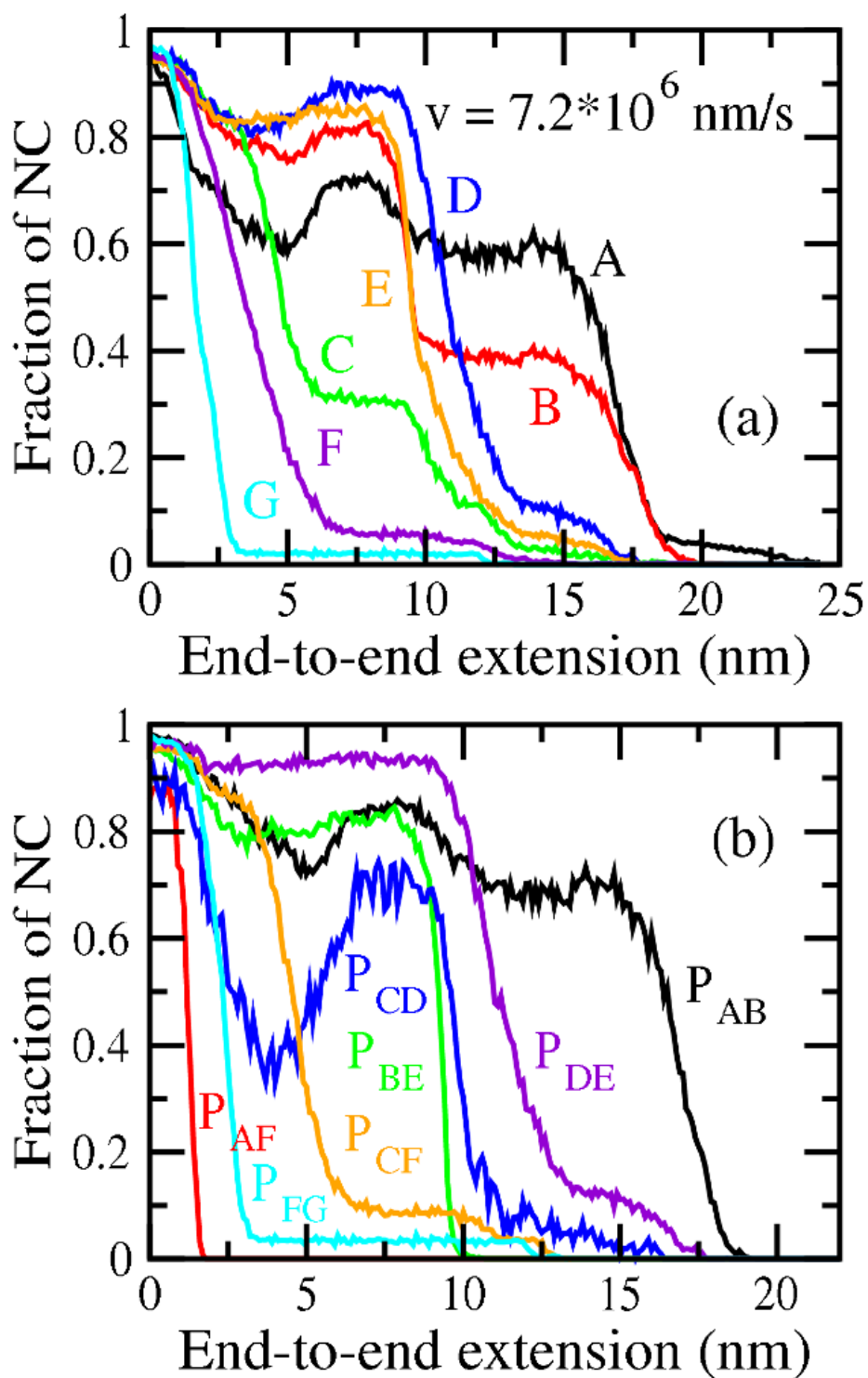


FIG. 4:

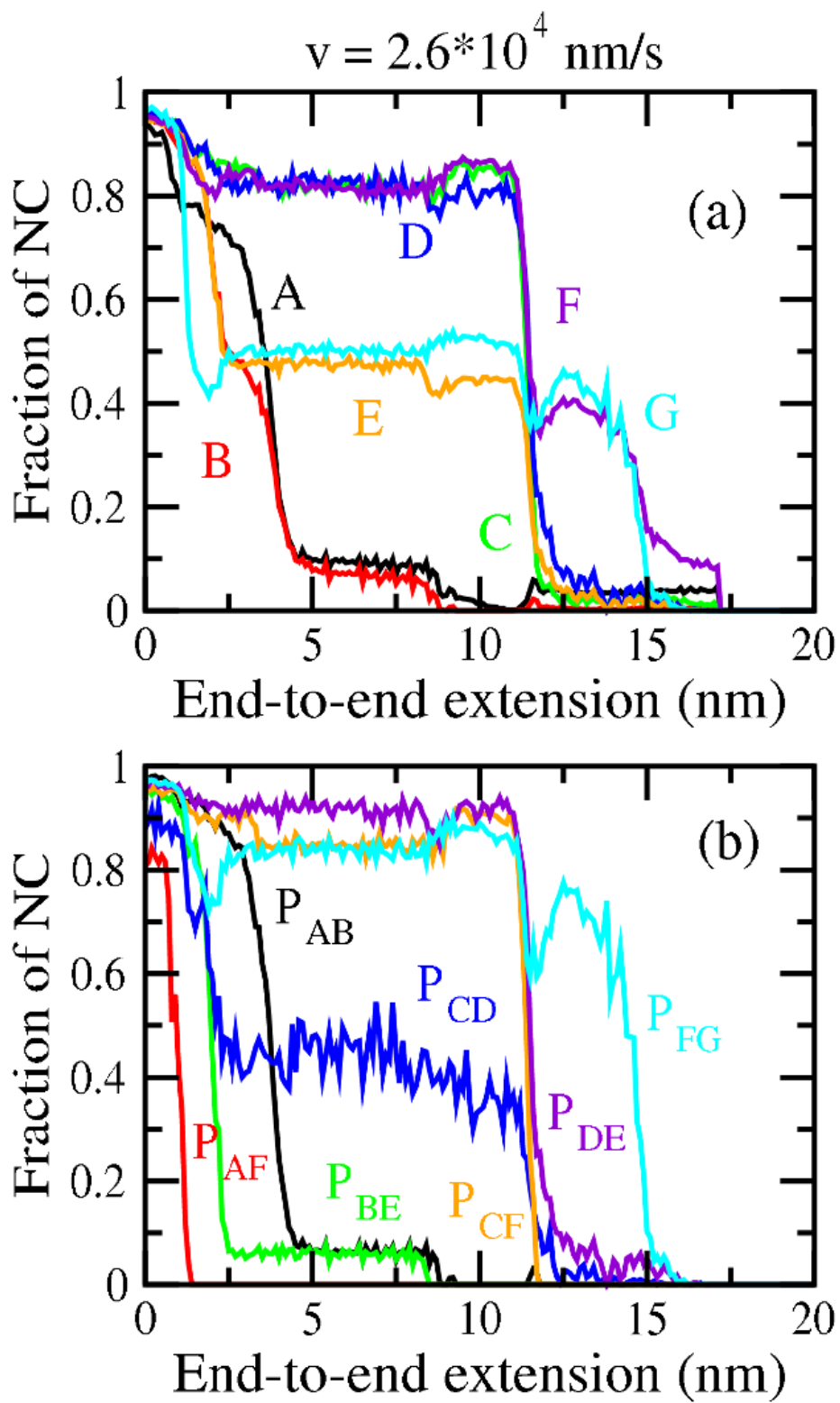
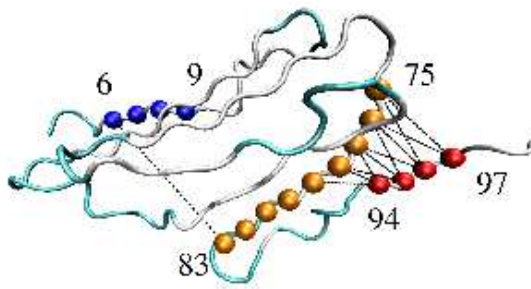
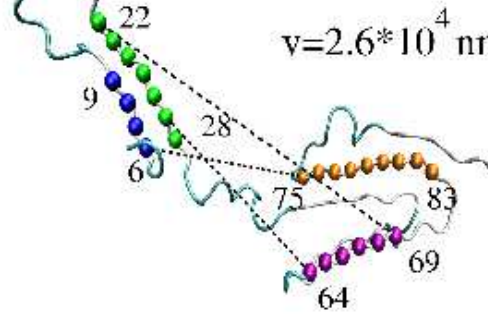


FIG. 5:

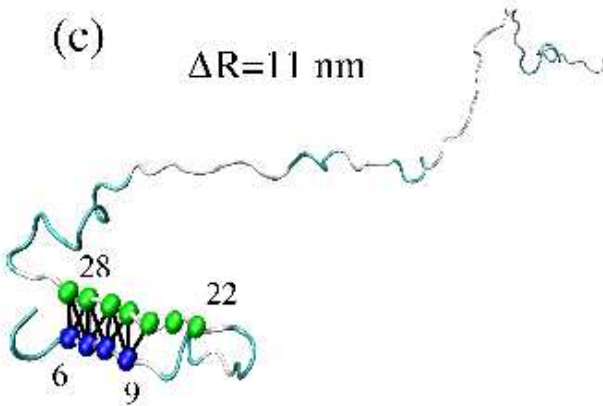
(a) $v=7.2 \cdot 10^6$ nm/s $\Delta R=2$ nm



(b) $\Delta R=2$ nm
 $v=2.6 \cdot 10^4$ nm/s



(c) $\Delta R=11$ nm



(d)

$\Delta R=11$ nm

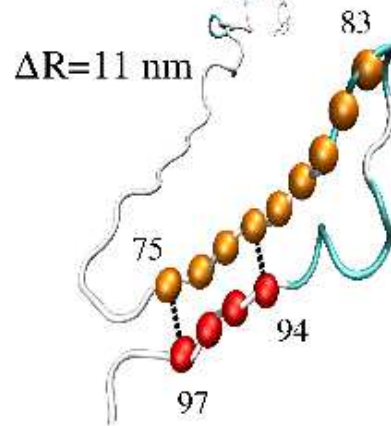


FIG. 6:

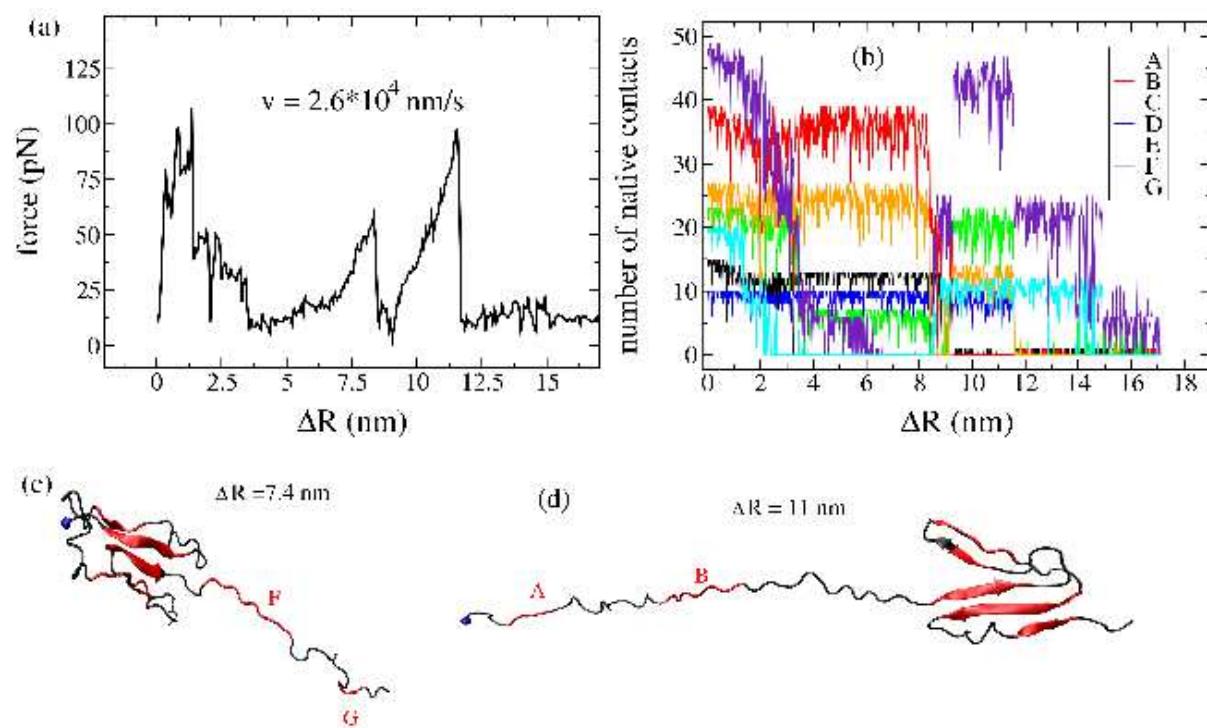


FIG. 7:

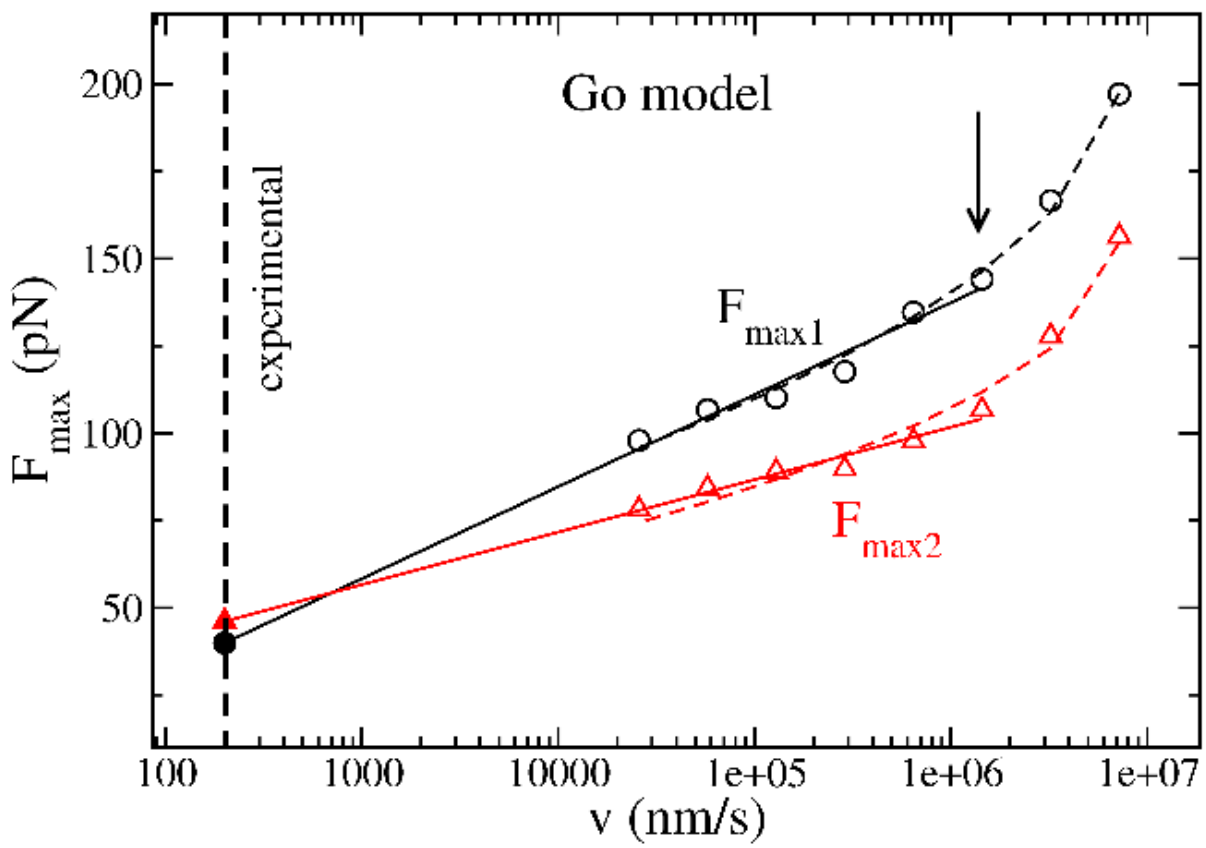


FIG. 8:

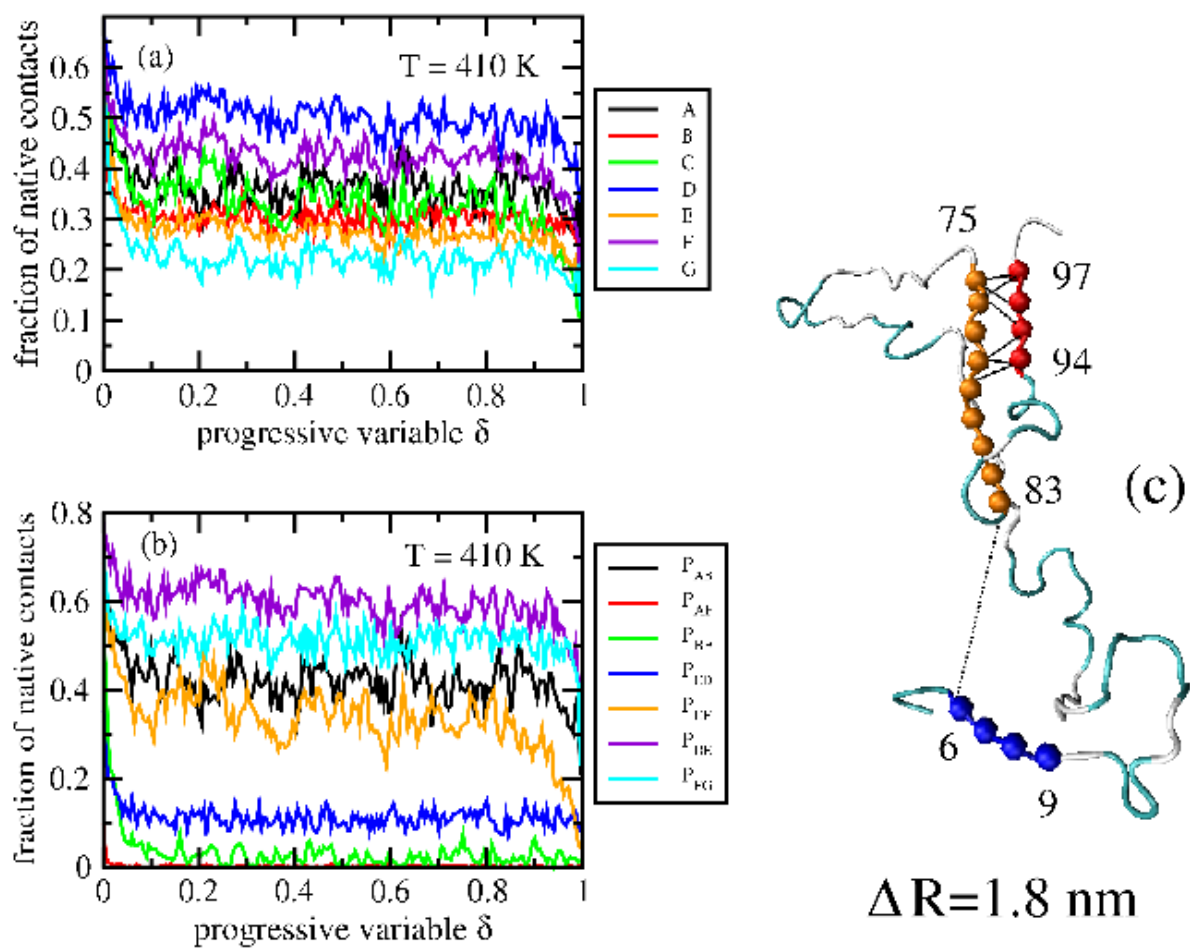


FIG. 9: